Pergamon

PII: S0191-8141(96)00074-0

Journal of Structural Geology, Vol. 19, No. 1, pp. 41 to 57, 1997

0191-8141/97 $17.00 + 0.00

Shear zones as a result of intraplate tectonics in oceanic crust: the example of the Basal Complex of Fuerteventura (Canary Islands)

CARLOS FERNANDEZ

Departamento de Geología, Universidad de Huelva, E21819-Palos de la Frontera, Huelva, Spain

RAMON CASILLAS and AGUSTINA AHIJADO

Departamento de Edafología y Geología, Universidad de La Laguna, E38206-La Laguna Tenerife, Canary Islands, Spain

VIRGINIA PERELLO

Departamento de Geología, Universidad de Huelva, E21819-Palos de la Frontera, Huelva, Spain

and

ALFREDO HERNANDEZ-PACHECO

Departamento de Petrología y Geoquímica, Universidad Complutense de Madrid, E28040-Madrid, Spain

(*Received* 7 *March* 1996; *accepted in revised form* 25 *August* 1996)

Abstract—Ductile shear zones affecting igneous rocks (pyroxenites, syenites, gabbros and carbonatites) belonging to the Basal Complex of the Island of Fuerteventura are described here. They develop typical mylonites with their cortege of structures and crystallographic fabrics. An evolution from brittle to ductile conditions has been recognized, and interpreted as being due to the ascent of alkaline magmas and related fluids and subsequent emplacement of weak rocks (carbonatites, syenites) along the shear zones. Local metamorphic changes favour the ductile behaviour *via* a reaction-enhanced softening mechanism. The shear zones are arranged in a nearly orthorhombic pattern. Kinematic criteria suggest an extensional tectonic scenario, with a bulk irrotational non-plane deformation. The long axis of the finite deformation ellipsoid is E–W and horizontal. The available data allow us to establish this deformation as being from the Late Oligocene to the Early Miocene. This is tentatively related to the plate-tectonics evolution and mantle anomalies in the northwestern corner of the African plate.

INTRODUCTION

Exploration of the oceanic crust is a powerful tool to understand the geometry and kinematics of the brittle and ductile structures within ocean ridges and transform faults, and therefore constitutes the key to knowledge of the tectonic evolution of plate boundaries. However, emerged portions of the oceanic crust are scarce and of small areal extent, making their importance invaluable. Fracture analyses carried out in selected areas, such as in Iceland (e.g. Gudmundsson, 1992; Fjäder *et al.*, 1994; Villemin *et al.*, 1994), can be cited as relevant examples of the study of the brittle behaviour in this context. Interesting data on the stretching of the deep crust at mid-ocean ridges have emerged from the study of the Deep Sea Drilling Project and the Ocean Drilling Program legs (e.g. Cannat *et al.*, 1991). A vast amount of structural data have been collected from the segments of oceanic lithosphere incorporated into continents during orogenies: the ophiolites. The Oman ophiolite (cf. Nicolas, 1989 for a review) and the Troodos Massif of Cyprus (Varga, 1991; Allerton and Vine, 1992; MacLeod and Murton, 1993) may be cited as two of the best-known cases in the world.

In contrast, little is known about intraplate tectonics in the oceanic lithosphere. From a petrologic point of view, the influence of the mantle hot spots in the oceanic crust is well established, and this has been used to deduce the position of euler poles and to compute relative velocities between plates (Minster and Jordan, 1978; Morgan, 1983; Müller *et al.*, 1993).

A complex tectonic scenario may be identified in the northwestern part of the African plate. At least from the Late Eocene, Africa converges towards the Eurasian plate. The Euler pole describing the relative motion of both plates is located to the southwest of the Canary Islands (e.g. Chase, 1978; Minster and Jordan, 1978; Argus *et al.*, 1989; Westaway, 1990). This causes a frontal convergence in the eastern and central Mediterranean, and a dextral, strike-slip transcurrent motion in the central-eastern Atlantic (the Gloria fault, Buforn *et al.*, 1988; Argus *et al.*, 1989). The presence of minor

continental blocks and ocean basins located between the continental masses of Africa and Eurasia led different authors to define this zone as a diffuse plate boundary (Vegas, 1985; Weijermars, 1988). Seismic evidence suggests that the African oceanic crust at the Central Atlantic may have been subjected to the same tectonic instability (Buforn *et al.*, 1988; Moreira, 1991). A further complexity results from the influence of a large region of upwelling in the upper mantle below the western Mediterranean and eastern Atlantic, which may account for some geochemical signatures of the Eastern Atlantic volcanic province (Hoernle *et al.*, 1995).

The Canary Islands belong to the Eastern Atlantic volcanic province, and are located within the African plate, not far from its diffuse boundary with the Eurasian plate. They represent an emerged area of intraplate oceanic crust (Stillman, 1987; Marinoni and Pasquarè, 1994; Neumann *et al.*, 1995). The archipelago lies close to the rifted north African continental margin, but it is considerably younger than the oceanic lithosphere in this area. The complex geological history may be partly a consequence of the plate tectonics scenario described above, and partly a result of a local intraplate tectonics (Marinoni and Pasquarè, 1994). In the present paper we describe two ductile–brittle shear zones affecting the older igneous series of the island of Fuerteventura. These shear zones accommodated important displacements (several hundred and perhaps even several thousand metres), and acted as ascent channels for mantle-derived magmas and fluids. The presence of ductile shear zones in Fuerteventura was first recognized and described by Casillas *et al.* (1994). The kinematic characterization of this deformation may be of relevance in the study of the recent tectonics of the African plate, and may contribute to a better knowledge of the behaviour of the oceanic crust in complex within-plate areas.

GEOLOGICAL SETTING

The Canary Islands are a group of volcanic islands and seamounts located on thick oceanic crust adjacent to the Atlantic-type continental margin of Africa (Fig. 1). From a geological perspective they constitute one of the more complex oceanic archipelagos in the world. Several successive magmatic periods led to the growth and emergence of these ocean islands, the process involving stages of partial destruction of the volcanic successions (Schmincke, 1982; Staudigel and Schmincke, 1984; Le Bas *et al.*, 1986; Coello *et al.*, 1991; Ancochea *et al.*, 1990, 1993, 1994).

Every island within the archipelago has its own geological history. The evolution process of Fuerteventura is the most complex and longest-lasting (Stillman *et al.*, 1975; Fúster *et al.*, 1980; Le Bas *et al.*, 1986; Coello *et al.*, 1991; Ancochea *et al.*, 1994). Fuerteventura forms part of the East Canary Ridge, together with Lanzarote and the Conception Bank. It is located on thick (more than 11 km) and strongly reworked oceanic crust (Banda *et al.*, 1981). Three main lithological units can be distinguished in Fuerteventura (Fig. 1).

(1) *The Basal Complex* consists of sea-floor sediments overlain by submarine volcanic and volcaniclastic sequences. The exposed sediments, Cretaceous in age, are part of the overturned limb of a concentric recumbent fold (Rothe, 1968; Robertson and Stillman, 1979a; Fúster *et al.*, 1980; Robertson and Bernouilli, 1982; Renz *et al.*, 1992). The volcanic series comprise breccias, hyaloclastites and pillow-lavas of basaltic to trachybasaltic composition. Bioclastic and volcaniclastic sediments of Middle to Late Oligocene age appear intercalated within the volcanic series (Fúster and Aguilar, 1965; Robertson and Stillman, 1979b). Large plutonic, and hypabyssal bodies intruded the sediments and volcanics. Following Stillman *et al.* (1975), Fúster *et al.* (1980), Le Bas *et al.* (1986), Stillman (1987) and Sagredo *et al.* (1989), three magmatic episodes can be recognized, including (i) an initial ultra-alkaline series comprising pyroxenites, amphibole-rich ultramafic igneous rocks, amphibole-bearing gabbros and syenites, cross-cut by syenite and carbonatite dykes, (ii) elongate, NNE–SSW trending bodies of gabbro and pyroxenite, and (iii) concentric patterns of gabbro and syenite ring-dykes. A dense basaltic dyke-swarm traverses the various lithologies. These dykes may be considered as the feeder conduits for rocks that form the submarine and subaerial growth of Fuerteventura and, in places, constitute more than 90 % of the exposed rock (Stillman *et al.*, 1975; Fúster *et al.*, 1980; Le Bas *et al.*, 1986; Stillman, 1987; Sagredo *et al.*, 1989). This obscures the continuity of contacts and structures within the Basal Complex.

(2) *A subaerial volcanic succession* of Miocene age comprises three large shield volcanoes, reconstructed from the disposition of the partly-eroded volcanic sequences (Coello *et al.*, 1991; Ancochea *et al.*, 1994).

(3) *A later subaerial volcanic succession*, contains intercalated beach-sediments (Meco and Pomel, 1985).

The initial ultra-alkaline series of Unit (1) are the lithologies affected by the shear zones. The more recent plutonics and the subaerial volcanic successions cut the shear zones, imposing temporal constraints to their activity. No evidence of ductile shearing has been found as yet in the intruded Cretaceous to Oligocene sediments and submarine volcanics. Therefore, this study is devoted to the description of the deformation affecting the older plutonics of Unit (1), the Basal Complex.

GEOMETRY AND KINEMATICS OF THE SHEAR ZONES

The shear zones in the ultra-alkaline plutonic rocks of the Basal Complex are unevenly distributed. Basaltic

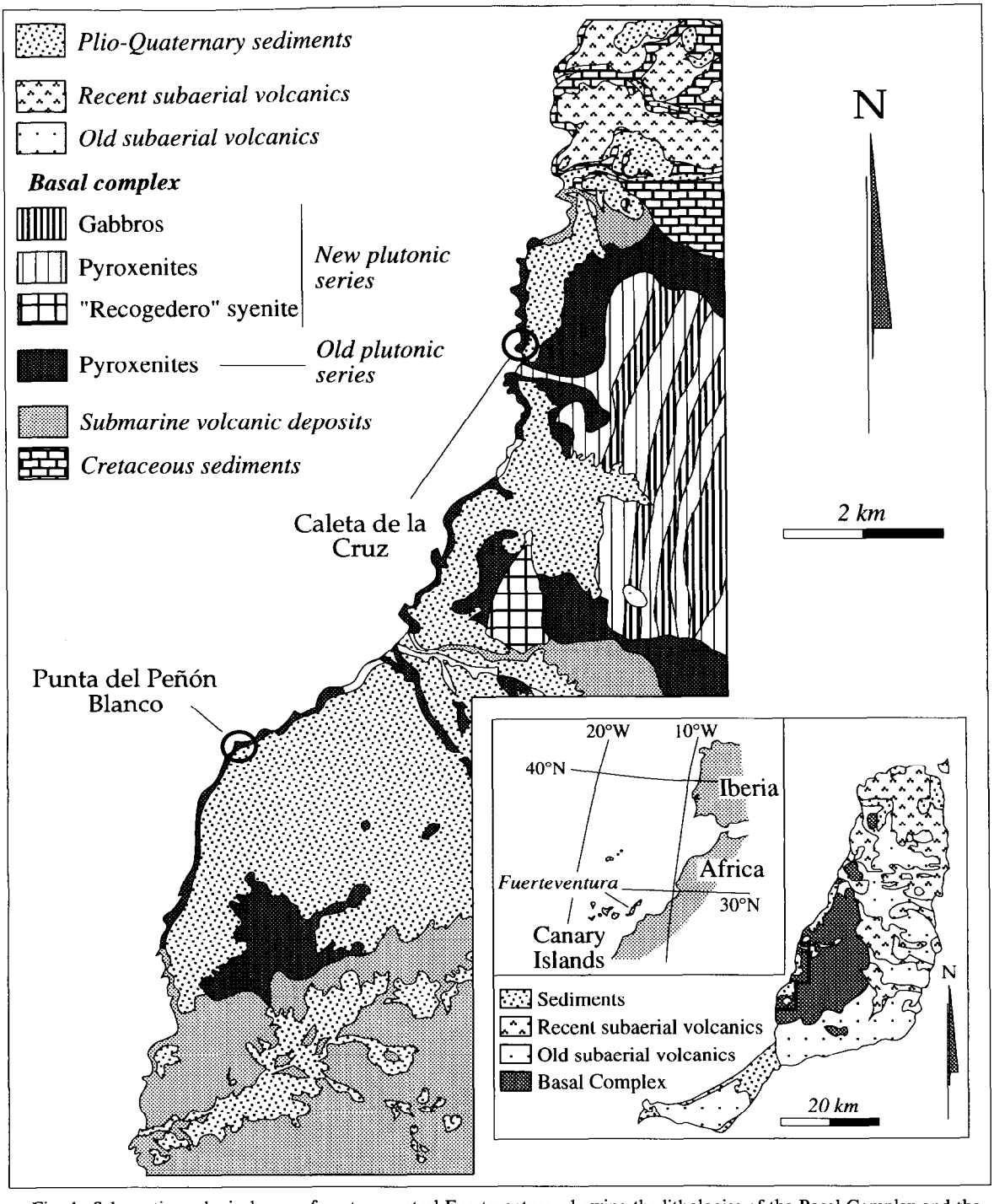

Fig. 1. Schematic geological map of western-central Fuerteventura, showing the lithologies of the Basal Complex and the location of the most important shear zones (Caleta de la Cruz and Punta del Peñón Blanco).

dykes disrupt the deformational structures and, in cases of large dyke densities, the shear zones are almost completely transposed. Exceptionally good exposures appear in the coastal cliffs and beaches, but the outcropping structures cannot be continued landwards due to the presence of the volcanic and sedimentary cover. In this work we describe the structures associated with two selected shear zones in the coastal section (Fig. 1): the Caleta de la Cruz and the Punta del Peñón Blanco shear zones. Here, the structures are clearly exposed and cleaned by sea-water abrasion and the density of the crosscutting dykes is moderate. The quality of the outcrops allowed the construction of orthogonal grids in the field with irregular, polygonal external contours. The side-length of the unit squares in the grids is 1 m. These grids were used as the reference frame for detailed geological mapping, a powerful tool to gain a complete geometric view of the shear zones. The analysis was

followed up by the use of conventional structural and petrologic techniques.

The Caleta de la Cruz shear zone (CCSZ)

This is a subvertical, NW–SE oriented shear zone (Fig. 2). A heterogeneous deformation affects a broad band (more than 10 m) of pyroxenites and syenites belonging to the initial ultra-alkaline series of the Basal Complex. The main structures originating in this shear zone are mylonitic foliation and lineation, curved-hinge folds, composite planar fabrics (C–S fabrics, Berthé *et al.*, 1979), lozenge-shaped blocks of undeformed pyroxenite, and minor discrete shear bands (Fig. 2). Apart from the heterogeneity of the deformation, the main characteristic of this zone is the brittle-to-ductile transition exhibited by the progressively developing structures. Near the external boundary of the shear zone, structures are brittle, with fractures fragmenting and displacing blocks of pyroxenite. This is observed also in the large lozenge-shaped blocks of pyroxenite within the CCSZ. The brittle structures are filled by carbonatite, whose appearance is strictly associated to the deformational structures. A complex metamorphic reaction (fenitization) between carbonatite and pyroxenite, which will be described in detail in the next section, results in an aggregate of phlogopite and diopside. Consequently, the ductility of the pyroxenite is highly enhanced locally, near the carbonatite intrusions. More continuous, straight and ductile shear bands appear in the inner part of the CCSZ. Here, a strongly foliated, fine-grained aggregate of calcite, phlogopite and diopside embraces residual fragments of pyroxenite. A reaction-rim of phlogopite–diopside is always present around these fragments. Reaction-rims are often stretched on both sides of a fragment, defining asymmetric tails (Fig. 3a & b) that recall the σ- and δ-structures of the porphyroclast systems in quartz–feldspar mylonites (Passchier and Simpson, 1986).

The mylonitic lineation is defined by elongate mica aggregates and shows a low to moderate plunge (Fig. 2a). This points to an important strike-slip component of displacement for the CCSZ. Kinematic criteria used to infer the shear sense in the CCSZ include (i) the asymmetric attitude of the foliation embracing the pyroxenite fragments (Figs 3a & 4a), (ii) the asymmetric tails of elongate reaction-rims around the pyroxenite fragments (Fig. 3a & b), (iii) the orientation and sense of shear exhibited by the minor shear bands and faults, (iv) the composite planar fabrics, (v) the preferred orientation of the calcite *c*-axis fabric (see later), and (vi) the orientation and asymmetry of mesoscopic folds affecting the mylonitic foliation (Figs 2a & 3b). In this case, the flow direction and flow sense are obtained following the method of Hansen (1971). All these indicate a dextral shear component with a subordinate down-throw of the northeastern block.

A second shearing episode deforms the previous structures. The new shear zone, with a thickness of 1 m, cross-cuts the southern boundary of the CCSZ. Basic dykes that had intruded the foliated carbonatites of the CCSZ are displaced and disrupted by this second episode

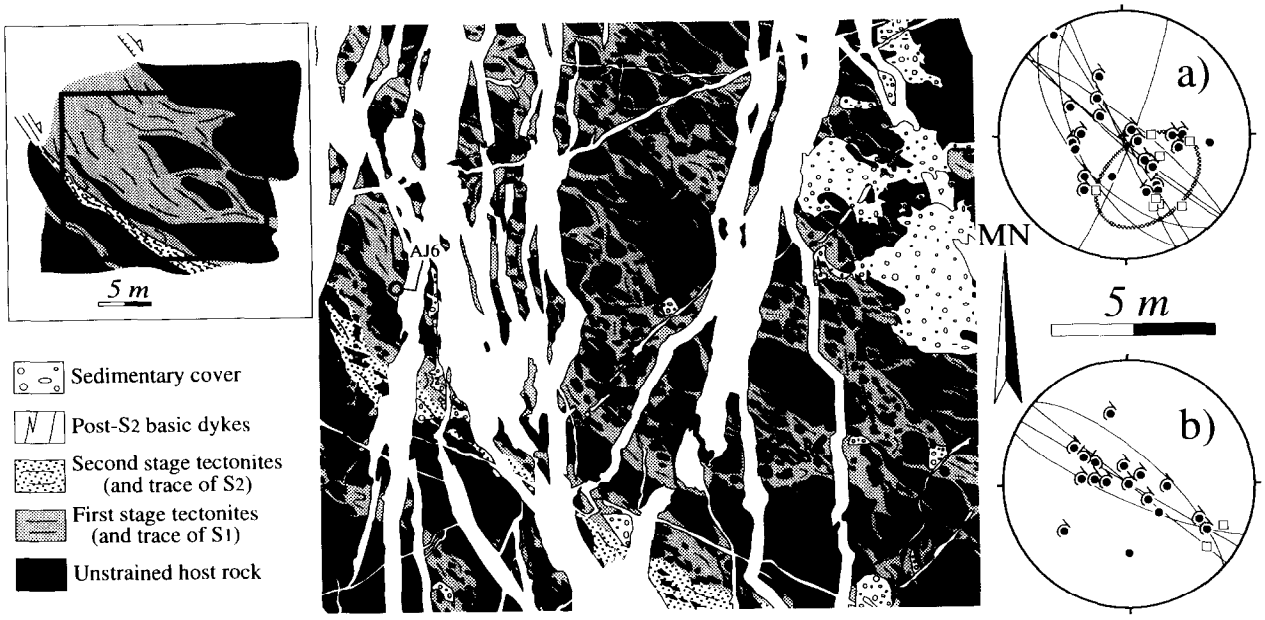

Fig. 2. Detailed geological map of the Caleta de la Cruz shear zone. This represents the best subhorizontal outcrop of this shear zone. The inset shows a sketch obtained after eliminating the late basic dykes. Sample AJ6, used in the texture analysis, is also located in the map. This (and most of the following figures) refer to the magnetic north (MN) as the mean deviation from the geographical coordinates appears negligible (Marinori and Pasquarè, 1994). (a) Structural data of the first deformational stage (great circles: foliation; open squares: mineral and stretching lineations; ellipse: area covered by the lineation poles; black dots: fold axes and sense of fold asymmetry). (b) Structural data of the second deformational stage; symbols as in (a). Spherical projections are equal area, lower hemisphere.

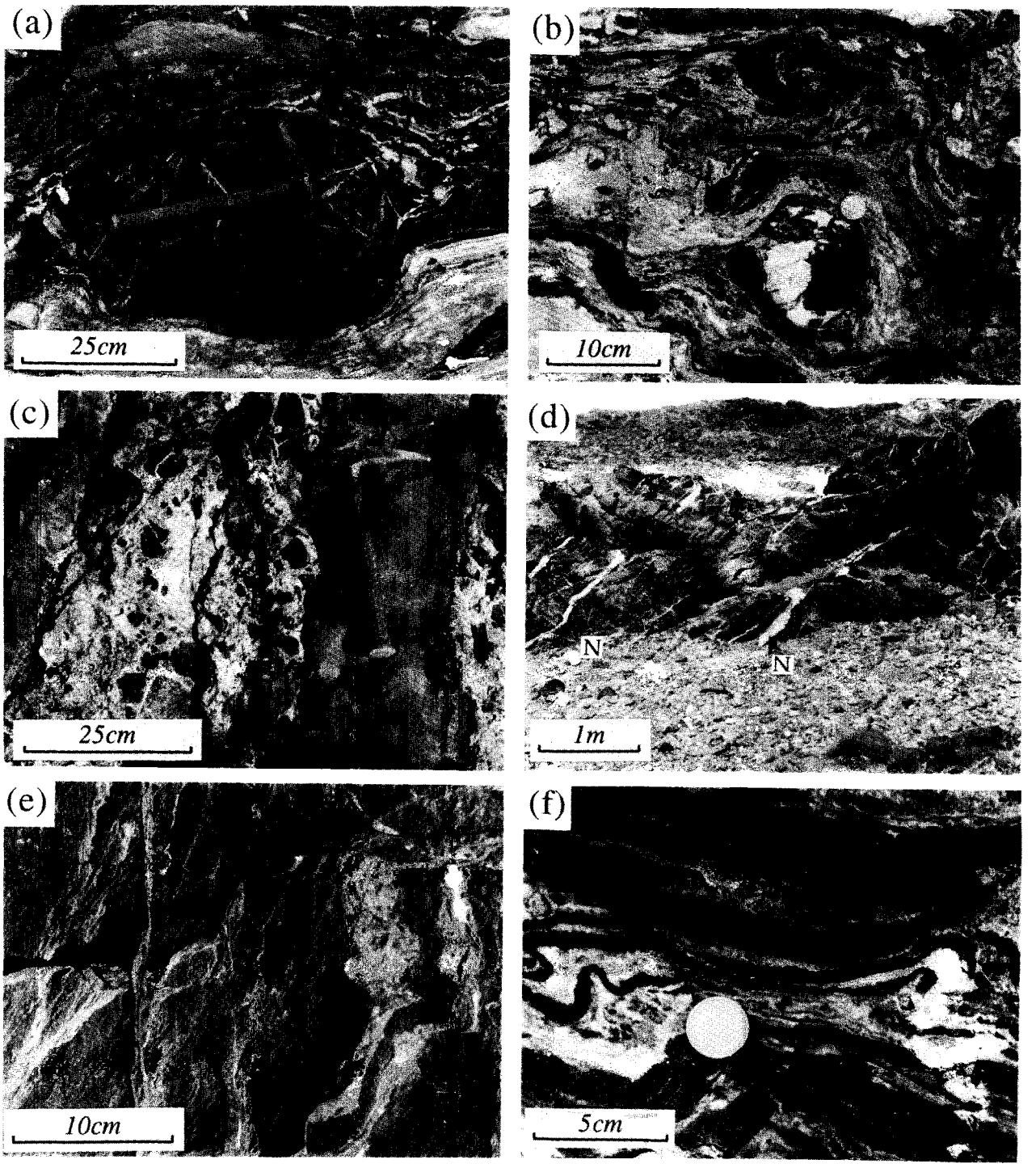

Fig. 3. (a) Pyroxenite block asymmetrically embraced by the mylonitic foliation composed of domains of recrystallized carbonatite (white) and domains of phlogopite ± diopside ± calcite (black). The pyroxenite block is contoured by a black reaction rim made of phlogopite and diopside. Caleta de la Cruz shear zone. ESE to the right of the photograph. (b) Folded mylonitic foliation with minor blocks of pyroxenite + syenite. Caleta de la Cruz shear zone. ESE to the right of the photograph. (c) Network of albitite in the Punta del Peñón Blanco area (type 1 veins). Hammer lies over a late, cross-cutting basic dike. (d) Pattern of type 2 and type 3 veins in the Punta del Peñón Blanco. Type 2 veins are filled by albitite and appear as thin and irregularly oriented veins. Type 3 veins are filled by white nepheline syenite (marked by N); they are thick and systematically dip to the left of the photograph (West). (e) Mylonitic lineation in the Punta del Peñón Blanco shear zone. ESE to the left of the photograph. (f) Curved-hinge fold in the Punta del Peñón Blanco shear zone. The folded layering is comprised of pre-and syn-kinematic basic dykes (black) and recrystallized carbonatite (white). ESE to the right of the photograph.

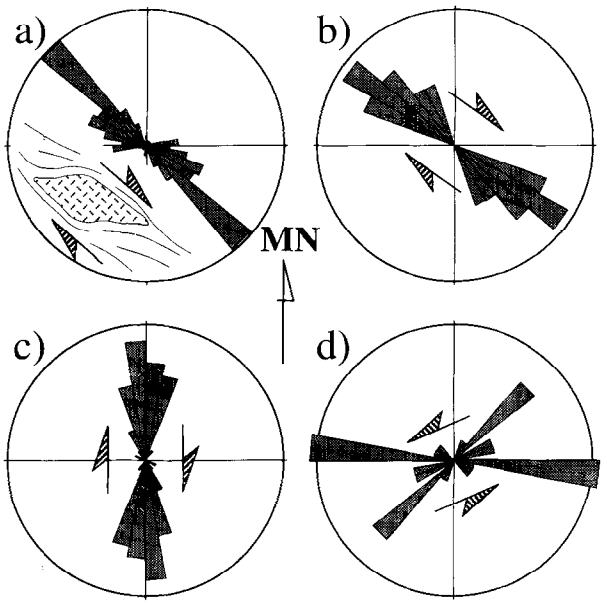

Fig. 4. Rose diagrams representing the traces of structural elements measured in the map of the Caleta de la Cruz shear zone. The frequency of the external perimeter is 30 %. (a) Traces of the first stage foliation ($n = 96$); the asymmetry of the diagram is explained as a consequence of the irregular distribution of the foliation embracing unstrained blocks in a dextral shear regime. (b) Traces of the second stage foliation ($n = 14$). (c) Traces of dextral shear bands ($n = 41$); (d) Traces of sinistral shear bands ($n = 22$).

(Fig. 5), indicating a horizontal displacement of more than 10 m in a dextral sense. The deformation associated with this shear zone caused a marked decrease in grain-size of the rock, as well as the elongation of the pyroxenite fragments. The kinematic pattern of this episode is not very different from that of the CCSZ, as deduced from the attitude of the mylonitic foliation and lineation and from the asymmetry of isoclinal intrafolial folds (Fig. 2b). Other kinematic criteria include the asymmetric shape of the disrupted basic-dyke fragments, the presence of tension gashes inclined with respect to the trend of the average foliation, the synthetic and antithetic shear bands, and the reorientation undergone by the earlier foliation in the vicinity of the newly-formed shear zone (Fig. 5).

The spatial association of both deformational episodes, together with the kinematic and metamorphic similarities between them, suggest a long-lived period of dextral ductile–brittle shearing with an intercalated stage of brittle behaviour and dyke intrusion.

The Punta del Peñón Blanco shear zone (PPBSZ)

This shear zone outcrops more than 7 km southwest of the Caleta de la Cruz (Fig. 1). A band of high ductile deformation with a thickness of around 40 m is located within a region of severely brecciated pyroxenite. A sudden decrease in the fracture intensity occurs on both sides of the brecciated area (Fig. 6a). Three types of veins fill the fractures in the brecciated pyroxenite:

Type 1. Irregularly impregnated areas which constitute a network of albitite (Fig. 3c).

Type 2. Albitite veins of cm-scale thickness, arranged in four systems with an approximate orthorhombic symmetry (Figs 3d & 6b).

Type 3. White nepheline syenite veins, with a marked unimodal preferred orientation (Figs 3d & 6c).

The PPBSZ is restricted to the ductile band located near the northern margin of the brecciated area, which becomes strongly deformed and even transposed (Fig. 7).

The albitite veins of the first two types described above are deformed by the ductile shear zone. However, the third type, of white syenite veins, systematically cross-cuts the ductile structures and appears only in the hanging-wall to the PPBSZ. They eventually affect the top of the main ductile band.

In Fig. 8, a selected region of the PPBSZ is shown in detail. As noted in the CCSZ with reference to the carbonatites, distinct lithological types are spatially related to the deformed area. These lithologies include carbonatite and dykes of grey nepheline syenite, which are scarce or absent in the ultra-alkaline unit outside the domains affected by the shear zones. Here we interpret these lithologies as intruded in relation to the activity of the shear zones. The dykes intrude the pyroxenite brecciated by the albitite network and veins. These dykes may extend by dozens of metres outside the boundaries of the PPBSZ (Fig. 7).

The mylonitic foliation has an average NW–SE trend. The plunge of the associated lineation approximates 40° to the SE (Figs 3e & 7c). Local places where the foliation trend departs from their average orientation are due to slight deflections around undeformed blocks of brecciated pyroxenite or nepheline syenite (Fig. 8). The mylonitic lineation is well developed in the grey nepheline syenites, where it is marked by the shape fabric of sanidine crystals and by the orientation of ribbons of sanidine and aggregates of aegirine–augite. Therefore, it constitutes a stretching lineation (Fig. 3e). In the carbonatites, which have an equigranular texture, the lineation is poorly defined, and the foliation is marked by occasional calc-silicate bands and alternating domains of fine- and coarse-grained carbonatite.

Kinematic criteria, some of which are clearly seen in the maps (Figs 7 & 8), are consistent with a dextral-normal sense of shear. These include: (i) the lateral displacement of the syenite and basic dykes, (ii) the asymmetric pattern of the mylonitic foliation around less deformed fragments, (iii) the asymmetric pressure-shadows around blocks of undeformed rock, (iv) the crystallographic preferred orientation of calcite (see later), and (v) the asymmetry of minor, curved-hinge folds (Fig. 3f), and their consistent spatial arrangement in relation to the mylonitic foliation and lineation (Fig. 7d), as deduced from the method of Hansen (1971).

To the south of the main ductile PPBSZ, several carbonatite bands deflect and displace grey syenite

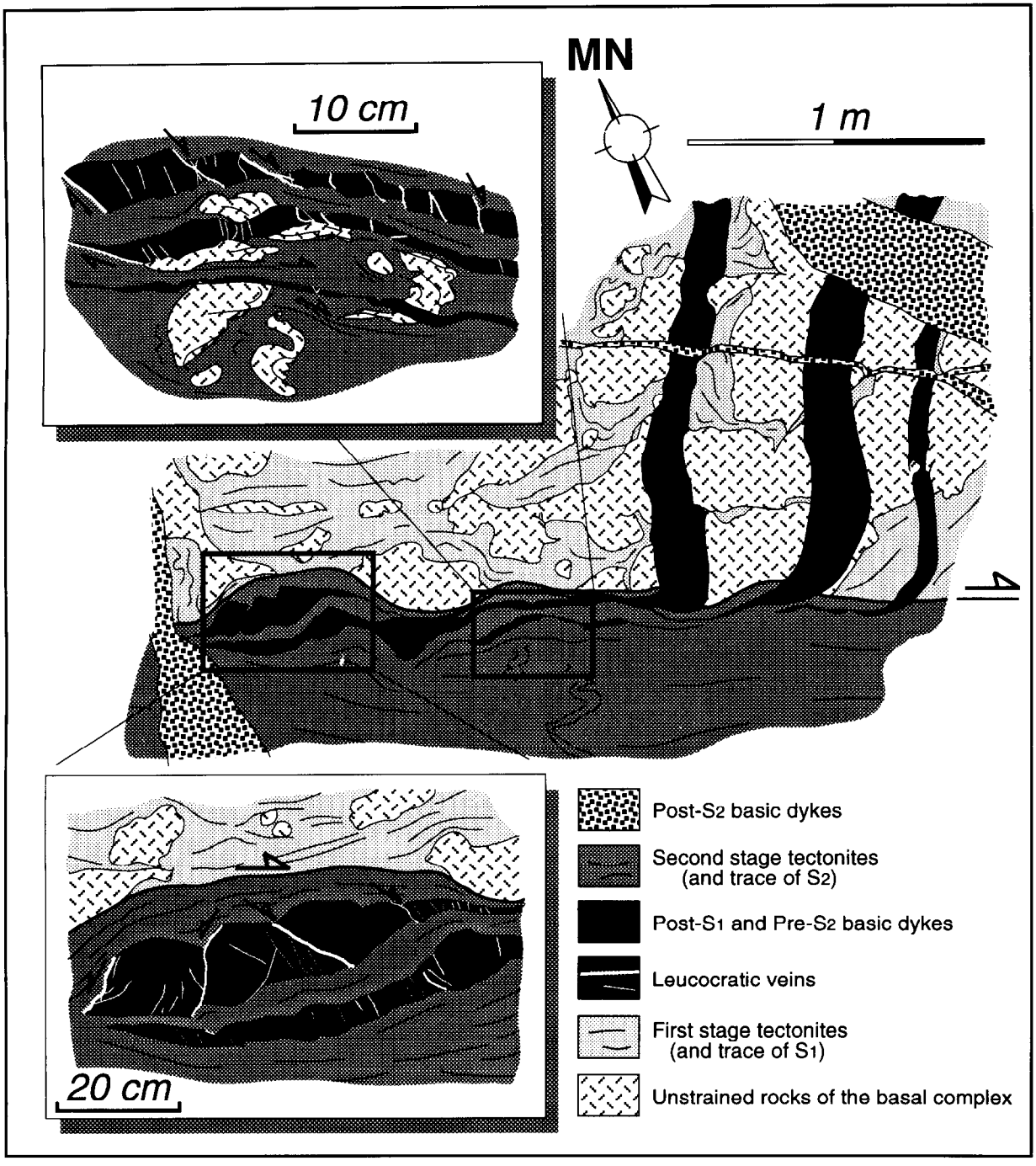

Fig. 5. Detailed sketch taken from field photographs, showing the effects of the second stage dextral shear zone on the basic dykes and first stage tectonites (Caleta de la Cruz shear zone). Insets depict the elongation of the basic dykes and their disruption by synthetic and antithetic fractures filled by leucocratic veins.

dykes (Fig. 7). The carbonatite within the bands is strongly foliated, and the syenite is more pervasively deformed when it approaches the bands. The strike-slip movement is dextral for the NW–SE and sinistral for the NE–SW oriented bands (Fig. 7a & b).

The large dykes of grey nepheline syenite located far from the main ductile shear zone are almost normal to the mylonitic lineation. As they approach the shear zone they become progressively rotated towards parallelism with the mylonitic foliation (Fig. 7e). The stretching and boudinage of the dykes generates a strongly developed planar–linear fabric.

The minimum displacement along the ductile band may be estimated according to the horizontal deviation of basic dykes in the margins of the shear zone (Fig. 8). A conservative extrapolation of this displacement to the

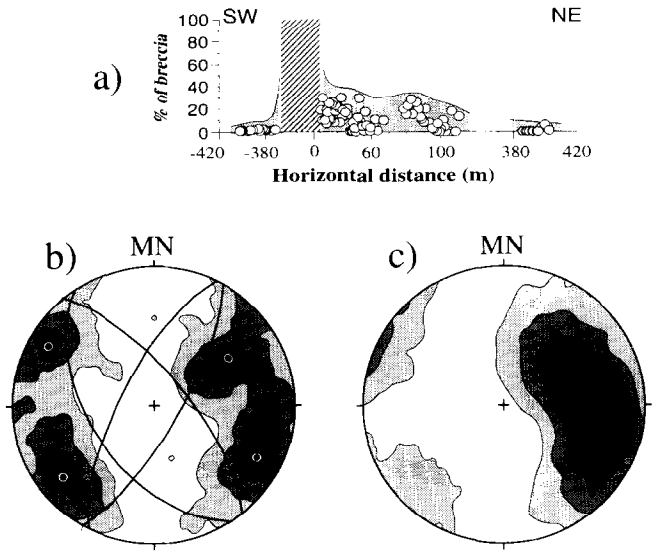

Fig. 6. Fracture intensity and orientation of the leucocratic veins in the Punta del Peñón Blanco area. (a) Linear percentage of brecciated areas with respect to the unstrained rock; the distance is measured in a direction normal to the boundaries of the ductile shear zone, the origin corresponding to the centre of the shear zone; the diagonal stripe pattern marks the area with 100 % breccia. (b) Contour diagram showing the orientation of the poles to the type 2, albitite veins; the maxima are the poles to the four great circles represented in the figure ($n = 339$). (c) Contour diagram showing the orientation of the poles to the type 3, nepheline syenite veins ($n = 72$). Contour diagrams are equal area, lower hemisphere projection, contoured after the Kamb method with $E = 3\sigma$, contour interval $= 2.0\sigma$.

entire band gives a net slip of more than 1 km. Considering the moderate thickness of the band (around 40 m), this is a quite large displacement, comparable to those measured in continental shear zones.

OPTICAL MICROSTRUCTURES, TEXTURES AND MINERAL CHANGES

The Caleta de la Cruz shear zone (CCSZ)

The pyroxenite blocks in contact with carbonatite develop a characteristic assemblage of phlogopite ± diopside ± magnetite ± apatite ± grossular/andradite garnet. Rocks in the deformed domains show unequivocal solid-state deformation microstructures, with a generalized reduction in the grain-size. The carbonatites filling fractures or located within pressure shadows around pyroxenitic blocks constitute unequant coarse-grained (2–3 mm) aggregates. Two conjugate sets of *e*-twins develop, although one set predominates over the other. Equant recrystallized grains (< 1 mm) appear at the grain boundaries or are located within discrete bands parallel to the foliation. Towards the inner part of the ductile CCSZ the grain-size is reduced (200–400 μm). Here the calcite crystals exhibit undulatory extinction, but they are almost free of deformation twins. The grains are slightly flattened with their long axes aligned parallel to the foliation. A crystallographic preferred orientation (also referred to as texture or crystallographic fabric in this paper) has been measured in the more deformed carbonatite aggregates (sample AJ6, for location see Fig. 2). All the textures in this paper were measured using the optical U-stage. The *c*-axis of calcite was determined as the pole to the great circle connecting 5 individually measured slow vibration directions, in accordance with the method by Turner and Weiss (1963). The result is shown in Fig. 9(a), with a high-density area near the normal to the foliation. Two unequally populated submaxima are present (I and II in Fig. 9a). The stronger one (maximum I) is deflected from the normal to the foliation in a sense opposite to the sense of the imposed shear, as deduced from other independent kinematic criteria. This texture compares well with the CT5 sample experimentally deformed by Schmid *et al.* (1987) under low-temperature, simple shearing conditions. Schmid *et al.* (1987) interpret this texture as a consequence of the simultaneous activity of *e*-twinning and *r*-slip. The virtual absence of twins in our sample is difficult to explain in this way, although it is possible that twinning was completed in a majority of crystals, as shown by Schmid *et al.* (1987) for some of the grains within their specimen CT5.

The second deformation stage produces an ultramylonite. A characteristic mineral and textural change is suffered by the displaced basic dykes. Far from the second-stage shear zone, they cross the trend of the first-stage foliation, and preserve an igneous ophitic texture. They show prismatic crystals of pyroxene and red biotite, enclosed by poikilitic plagioclase. An important metamorphic–metasomatic process gives rise to an assemblage of green biotite + grossular/andradite garnet + sphene + magnetite + analcite + epidote/clinozoisite + calcite. As the dykes rotate towards parallelism with the second-stage shear zone margin, the garnet is fragmented and stretched to generate trails of porphyroclasts within a very fine-grained matrix composed of grossular/andradite garnet + green biotite + sphene + albite + analcite + carbonates + magnetite. As described above, tension gashes and discrete shear bands cross-cut the dyke fragments within the shear zone. The mineral assemblages filling the veins are similar to those described for the matrix of the deformed dykes, and include analcite + calcite +

Fig. 7. Geological map of the coastal outcrop of the Punta del Peñón Blanco shear zone. The basic dykes cutting the ductile structures are not represented in this figure. The marked area corresponds to the detailed map of Fig. 8. (a) Dextral and (b) sinistral shear bands to the west of the main ductile shear zone. (c) and (d) Structural data of the main ductile shear zone. The area with a grey pattern in (d) indicates the position of the mineral and stretching lineations. Legend for (a)–(d): great circles, mylonitic foliation; open squares, mineral and stretching lineation; black dots, fold axes and sense of fold asymmetry. (e) Nepheline syenite dykes to the west of the main ductile shear zone; the bold great circle represents their orientation in the centre of the map, and the dashed arrow marks their progressive reorientation towards the ductile shear zone. Spherical projections are equal area, lower hemisphere. Samples R1, 425 and 442, analyzed for crystallographic preferred orientation, are also located in the map.

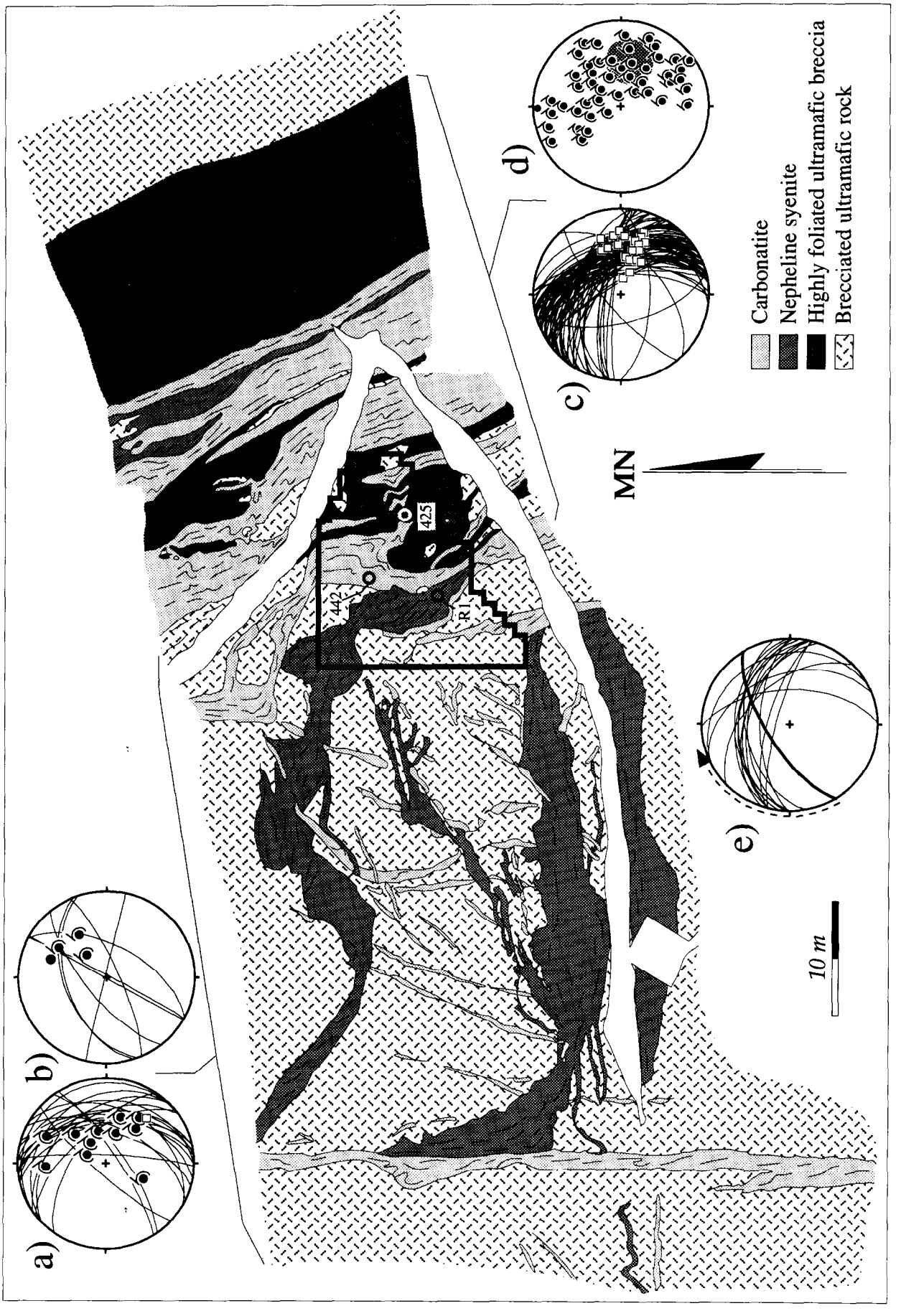
a)
b)
c)
d)
e)
MN
10 m
425
442
R1
Carbonatite
Nepheline syenite
Highly foliated ultramafic breccia
Brecciated ultramafic rock

Fig. 7.

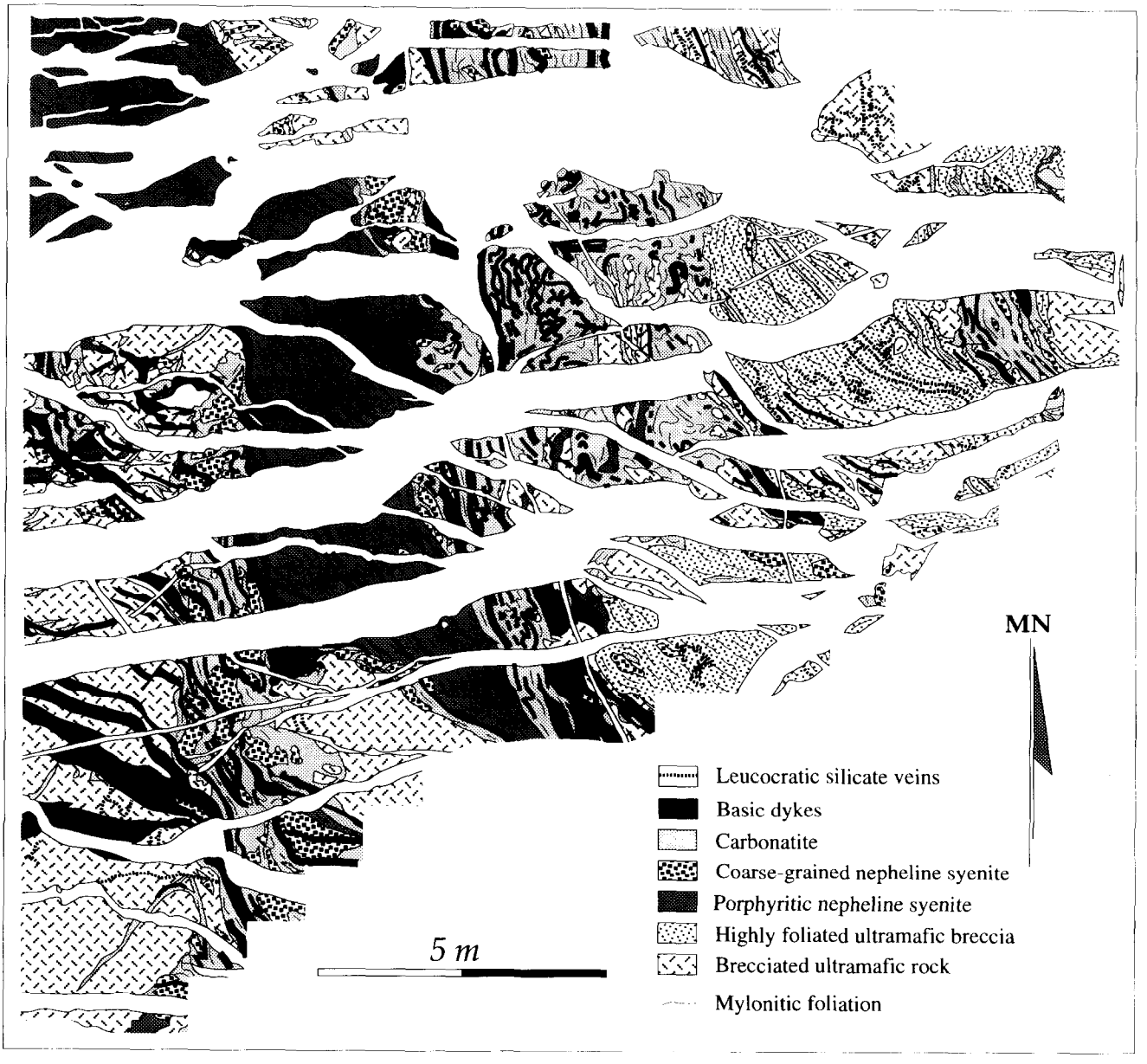

Fig. 8. Detailed geological map of the ductile shear zone in the Punta del Peñón Blanco (for location see Fig. 7).

garnet + green biotite. This strongly suggests a synchronous development of these structures with respect to the shear activity, and favours their use as kinematic criteria.

The fabrics of the first-stage deformation are heavily recrystallized within the second-stage shear zone. The metamorphic mineral assemblages are also changed to grossular/andradite garnet ± Sr-rich epidote/clinozoisite ± idocrase ± magnetite analcite ± Sr-rich allanite ± calcite.

The Punta del Peñón Blanco shear zone (CCSZ)

The microstructural study was focused on the grey nepheline syenite dykes, carbonatites and foliated pyroxenite breccias.

The nepheline syenite is essentially composed of sanidine, aegirine–augite and nepheline. When undeformed it presents an igneous porphyritic texture with prismatic sanidine and aegirine–augite phenocrysts in a matrix of nepheline, sanidine and aegirine–augite. The long axes of the sanidine phenocrysts have an average length of approximately 5 mm. With the increase in ductile deformation, the grain-size is reduced. Nepheline, with abundant undulatory extinction and subgrain boundaries, acquires a strong crystallographic preferred orientation (sample R1, for location see Fig. 7), with a single-maximum, *c*-axis fabric parallel to the mineral lineation (Fig. 9d). Recrystallization must proceed in an anhydrous environment as deduced from the mineralogy of the deformed rocks, devoid of hydrous minerals such as micas or amphiboles. Sanidine also shows subgrain boundaries and an interesting texture, with the α-axes of the optical indicatrix located in a single maximum close to the mineral lineation, the β-axes forming an incomplete girdle parallel to the foliation, with a maximum

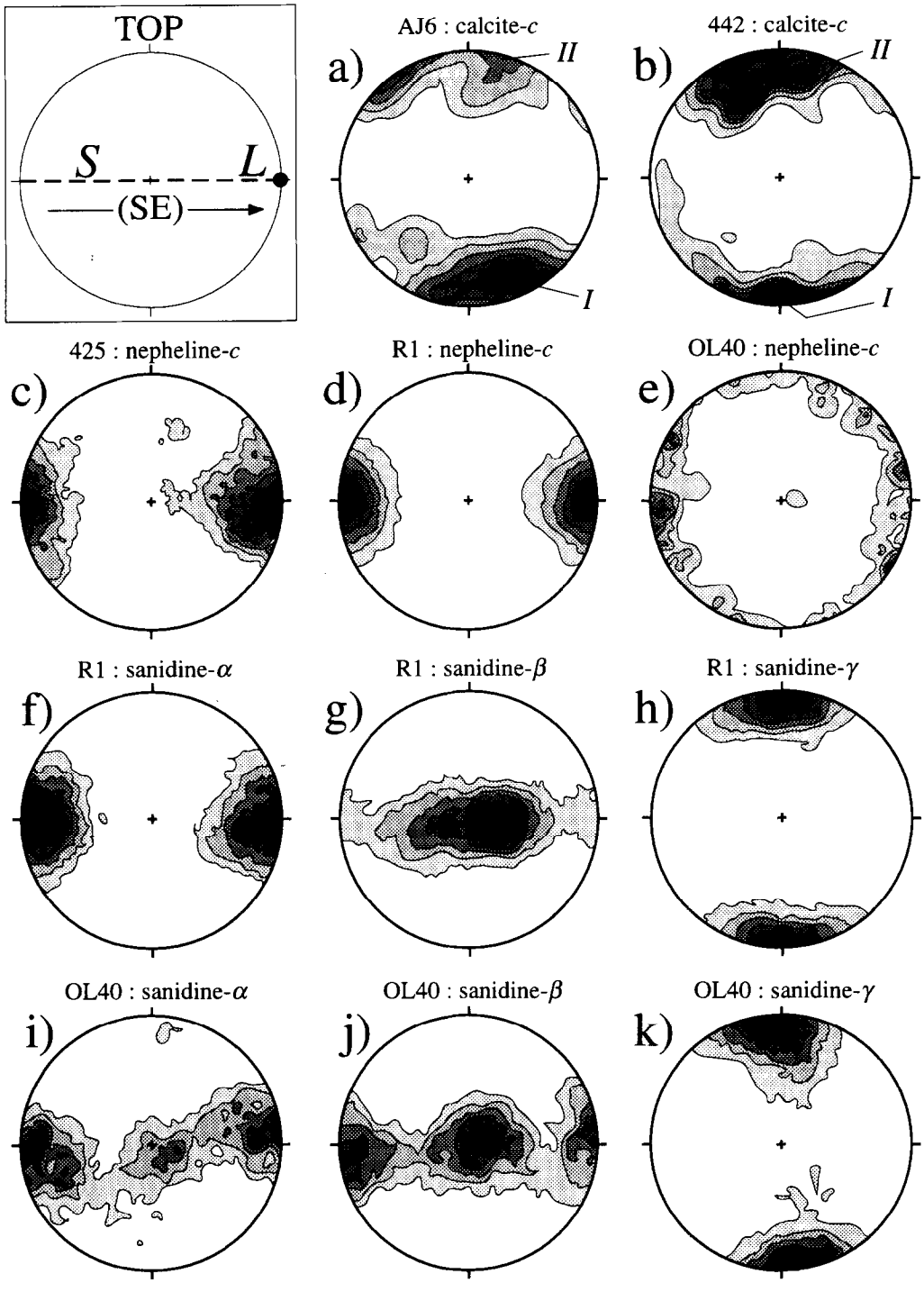

Fig. 9. Crystallographic preferred orientations in deformed rocks of the Basal Complex. The inset depicts the orientation of the structural co-ordinate system: foliation (*S*) and lineation (*L*). Shear sense is dextral for all diagrams. Equal area, lower hemisphere projection. Density calculation after the step-function, except for (a) and (b) where a spherical Gaussian function was used instead. Contouring after the Kamb method with $E = 3\sigma$. (a) *c*-axis fabric of calcite in a carbonatite from the CCSZ. Contour interval (c.i.) $= 1.2\sigma$. Number of measured crystals (n) $= 144$. (b) *c*-axis fabric of calcite in a carbonatite from the PPBSZ; c.i. $= 1.4\sigma$; $n = 232$. (c) *c*-axis fabric of nepheline in a deformed pyroxenite breccia from the PPBSZ; c.i. $= 1\sigma$; $n = 204$. (d) *c*-axis fabric of nepheline in a deformed syenite from the PPBSZ; c.i. $= 2.5\sigma$; $n = 120$. (e) *c*-axis fabric of nepheline in a deformed syenite from a shear zone to the north of the CCSZ; c.i. $= 4\sigma$; $n = 103$. (f) to (k) Sanidine fabrics showing the orientation of the optical indicatrix axes in syenites from the PPBSZ (f–h) and a shear zone to the north of the CCSZ (i–k). (f) c.i. $= 1\sigma$; $n = 134$. (g) c.i. $= 1.5\sigma$; $n = 134$. (h) c.i. $= 2.2\sigma$; $n = 134$. (i) c.i. $= 0.5\sigma$; $n = 120$. 0) c.i. $= 0.7\sigma$; $n = 120$. (k) c.i. $= 1\sigma$; $n = 120$.

normal to the lineation, and the γ-axes coinciding with the pole to the foliation (Fig. 9f–h). The prismatic phenocrysts of sanidine undergo a reorientation with their long-axis parallel to the trend of the mylonitic foliation. Kinematic criteria are abundant in these phenocrysts (now porphyroclasts), and include sheared and asymmetrically detached parts of crystals, bookshelf sliding, and the asymmetric pattern of the foliation embracing large sanidines. They typically show a core–mantle structure produced by dynamic recrystallization. The average size of the newly recrystallized crystals is 200 to 300 μm. As deformation increases, recrystallization pervades the whole crystal, which is stretched to give a polycrystalline ribbon. Phenocrysts of aegirine–augite are also transformed into elongate polycrystalline domains parallel to the mylonitic lineation, but no signs of plastic deformation can be observed within individual crystals.

The mineral composition of the undeformed carbonatite is seldom preserved and consists of an aggregate of large (up to 2 cm) crystals of calcite, phlogopite and sanidine. In areas of low to moderate deformation, the carbonatite changes to a heterogeneous aggregate of calcite (up to 1 cm in size) with a metamorphic microstructure characterized by straight grain boundaries meeting at 120°. Ore minerals are concentrated along grain boundaries and planes of cleavage. A slight bending of the phlogopite lattice is also clear. Within more deformed areas, the calcite crystals show a core–mantle microstructure, with the growth of newly-recrystallized, equant crystals (200–400 μm). The host crystals developed undulatory extinction and two conjugate sets of deformation twins. Progressively, the recrystallized grains pervade the host crystals, which remain as flattened relics with aspect ratios of 2–3:1 in a section normal to the foliation and parallel to the lineation. Eventually, the dynamic recrystallization affects the whole aggregate, resulting in an equigranular (400 μm) mosaic of calcite, with undulatory extinction, subgrain boundaries and deformation twins. The calcite-texture obtained in this strongly deformed rock (Fig. 9b: sample 442, see Fig. 7 for location) is asymmetric with respect to the structural co-ordinate system. As in the CCSZ, two sub-maxima develop (I and II in Fig. 9b), with the more populated one inclined to the foliation normal in a sense opposite to the external shear sense. Simultaneous activity of *e*-twinning and *r*-slip is again proposed to account for this texture (Schmid *et al.*, 1987). Within the pressure shadows or other protected regions, the calcite forms a polygonal mosaic of large crystals, with grain boundaries meeting at 90°.

The brecciated pyroxenite was severely deformed to give a foliated rock with a pervasive tectonic banding. This banding is composed of alternating white and dark bands. The heterogeneous character of the deformation in the PPBSZ is clearly seen since the banded domains often show clear-cut contacts with respect to undeformed blocks of brecciated pyroxenite (Fig. 8). An equigranular aggregate of sanidine, albite and nepheline constitutes the white bands. It results from the transposition of the albitite veins and network. Some albitite veins exhibit isoclinal folds, with the tectonic banding as axial plane; other were stretched to generate pinch and swell structures and fish-mouth boudins. The crystallographic preferred orientation of nepheline is quite strong (sample 425, see Fig. 7 for location), with a single maximum of nepheline *c*-axes parallel to the mylonitic foliation (Fig. 9c). This strong fabric is due to the considerable solid-state deformation suffered by these bands. Similar nepheline *c*-axis fabrics were obtained by Fairbairn (1941) and Sturt (1961). The foliation in the dark bands is defined by the preferred orientation of biotite and diopside. Kinks and mica-fishes are the main microstructures in the biotite. The diopside shows no evidence of plastic intracrystalline deformation.

Textures in other minor shear zones

Nepheline syenites affected by other shear zones to the north of the CCSZ were also analyzed. The aim of this study is to show the homogeneity of the deformation mechanisms throughout the entire Basal Complex, with special reference to the textures in sanidine and nepheline.

Figure 9 (i–k) shows the axes of the optical indicatrix of sanidine composing more than 60 % of the matrix in a sample of a deformed syenite, 15 km to the north of the CCSZ (sample OL40). This shear zone is very heterogeneous and the deformation structures are not as strong as in the CCSZ or PPBSZ, suggesting lower strains. The α- and β-axis fabrics delineate a single girdle which is slightly oblique with respect to the foliation trace, the deflection being described by a counter-clockwise rotation around an axis normal to the stretching lineation and included within the mylonitic foliation. This counter-clockwise deflection is contrary to the imposed shear sense indicated by the meso- and microstructural criteria. Two maxima are discernible within both girdles, one of them normal to the mylonitic lineation, the other at 5–10° from it. The γ-axis fabric consists of a single maximum located at 5–10° counter-clockwise from the pole to the foliation plane. These results are similar to the fabrics of sanidine in the syenites of the PPBSZ (Fig. 9f–h). However, in the PPBSZ the fabrics are symmetrical with respect to the finite strain reference axes. Statistical measurement of the optic axial angles in sanidine, which is around 50° here and in the PPBSZ, indicates that it is high sanidine (e.g. Smith and Brown, 1988). In this case, the γ-axis maximum implies a strong disposition of the (001) planes near the foliation trace, with [001] normal to it. No accurate transmission electron microscopy analysis of the operative slip-systems was conducted in this work, and several problems are associated with the direct interpretation of fabric diagrams in terms of slip systems, as shown by Wenk and Christie (1991). In spite of these difficulties we suggest that (001) could have been an

important slip plane in the plastic behaviour of sanidines in the Basal Complex of Fuerteventura. This coincides with the results obtained by Willaime *et al.* (1979) and Scandale *et al.* (1983) on experimental grounds, and Sacerdoti *et al.* (1980) in the study of naturally deformed K-feldspar.

The nepheline constitutes a mere 10–15 % of the matrix. The nepheline *c*-axis fabric (Fig. 9e) is weaker compared to that exhibited by sanidine, and it shows a single girdle parallel to the plane containing the mylonitic lineation and the normal to the foliation. The main maximum within the girdle is deflected in a counter-clockwise sense from the stretching lineation. This fabric is weaker and quite different to the nepheline fabric in the PPBSZ (Fig. 9c & d).

Crystals of sanidine and nepheline in the matrix constitute an anhedral framework, and their microstructures are indicative of intracrystalline plasticity. Therefore, the systematic asymmetry between crystallographic axes of sanidine and nepheline and finite strain axes may be explained in the same manner as for quartz and calcite crystallographic fabrics; i.e. as being due to the presence of a rotational component in the flow (Law, 1990). Dextral simple shearing is deduced for this minor shear zone from other kinematic criteria. The physical process by which the sanidine and nepheline lattices rotate towards the pattern shown in Fig. 9 (e) and (i–k), under a component of dextral simple shear, is unknown and is beyond the scope of this work. However it seems reasonable to assume that with the increase in the shear strain, the textures become stronger and acquire a marked symmetry (Fig. 9c, d & f–h).

Deformation conditions

The mineral changes which took place within the carbonatites in contact with the other lithologies allow a preliminary estimation of the temperature conditions during the deformation. Two stages of skarn formation are involved in the process. The first stage resulted in metasomatic calc–silicate columns. Mineral assemblages are dominated by garnet + diopside. The pyroxenites and brecciated pyroxenites are transformed into aggregates of diopside ± garnet phlogopite ± apatite ± magnetite ± sulphides. The second stage is preferentially located along fractures, where a considerable change in the previous assemblages has occurred. The diopside is replaced by serpentine and green biotite, whereas the garnet is consumed to give another colorless garnet or an assemblage of epidote/clinozoisite ± albite ± calcite.

According to field and geochemical criteria, the thickness of volcanic materials overlying the ultra-alkaline series during activity of the shear zones can be estimated as 3 km (Javoy *et al.*, 1986). This implies a lithostatic pressure of around 1 kbar. If the fluid pressure is considered to be equal to the lithostatic pressure, the assemblage of diopside + phlogopite + grossular/andradite garnet, in the absence of wollastonite, suggests a temperature of 500 °C for the first metasomatic stage (Fig. 10, point A). The assemblages of the second stage imply an evolution to lower temperature (around 400 °C) and P_{CO_2} (Fig. 10, point B).

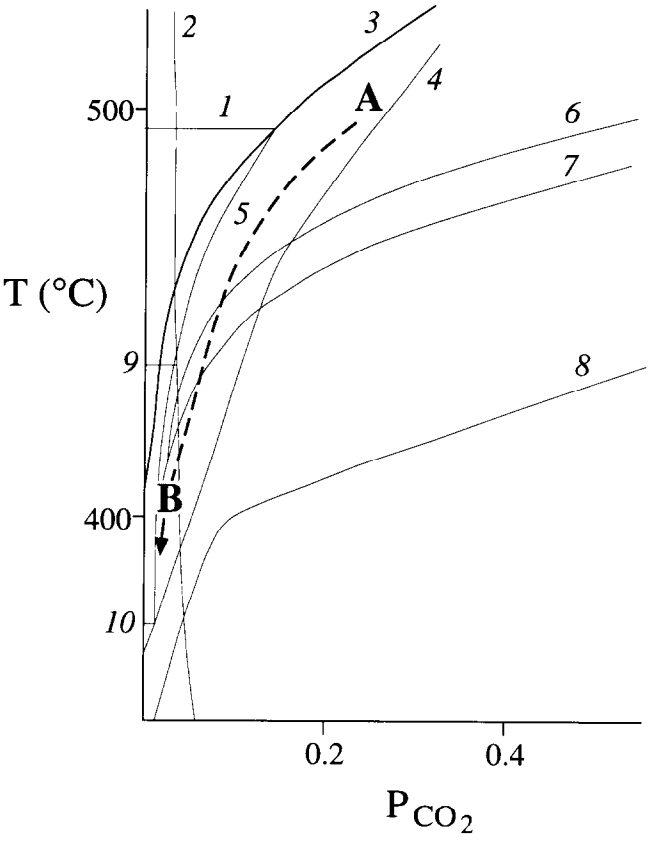

Fig. 10. T–P_{CO2} diagram (lithostatic pressure = 1 kbar). The main reactions in the system KCMAS (H_2O–CO_2) and CAS (H_2O–CO_2) are represented (following Taylor and Liou, 1978). 1: Grossular + Quartz = Anorthite + Wollastonite; 2: Zoisite = Anorthite + Calcite; 3: Calcite + Quartz = Wollastonite; 4: Quartz + Calcite + Magnetite = Andradite; 5: Grossular = Anorthite + Calcite + Quartz; 6: Tremolite + Calcite + K-Feldspar = Diopside + Phlogopite; 7: Tremolite + Calcite + Quartz = Diopside; 8: Rutile + Calcite + Quartz = Sphene; 9: Zoisite + Quartz = Anorthite + Grossular; 10: Prehnite = Clinozoisite + Grossular + Quartz. Also shown are the interpreted conditions for the first (A) and for the second (B) metamorphic stages.

DISCUSSION

The shear zones affecting the Basal Complex of Fuerteventura show clearly the activity of plastic intracrystalline mechanisms (dislocation glide and creep and mechanical twinning). Calcite, nepheline and, to a lesser extent, sanidine and biotite/phlogopite, are the mineral phases where the microstructures and textures of plastic deformation are best developed. Pyroxene and amphibole do not exhibit unequivocal plastic intracrystalline features. This fact conditions the distinct rheological behaviour in the shear zones. A classification of rock types from least to most competent might be as follows: carbonatite, nepheline syenite, brecciated pyroxenite, basic rock of dykes, pyroxenite. The competence con-

trasts result in a wide variety of structures, as illustrated in this work. These structures demonstrate ductile or brittle–ductile behaviour. The temperature within the shear zones reaches 400–500 °C, and is probably higher than the temperature in the pyroxenite host rock. Carbonatite melts and related alkaline fluids were channelled through the shear zones and are the only local heat source available to generate the observed thermal anomaly. However, the increase in temperature cannot alone explain the ductile behaviour. The host rock is essentially composed of pyroxene and amphibole, and temperatures well above 500 °C are necessary to promote plastic deformation in these strong minerals (e.g. Mercier, 1985). A process of whole mineral transformation in the host rock, including reaction-enhanced softening (White and Knipe, 1978), is favoured here. Within the shear zones, weak plastic minerals, such as calcite, nepheline, sanidine, and phlogopite, replace strong pyroxene and amphibole. Therefore, the emplacement of carbonatite and syenite together with the metamorphic changes in the pyroxenite, which becomes a phlogopite-rich rock, is a convincing mechanism to account for the transition from the brittle to the ductile regime.

The syenites and carbonatites were emplaced between 21 and 30 Ma according to Le Bas *et al.* (1986) and Cantagrel *et al.* (1993). The complexes of gabbro and syenite ring-dykes, which were not affected by the shear zones, were emplaced at 14.6 to 20.8 Ma before present (Abdel-Monem *et al.*, 1971; Grunau *et al.*, 1975; Le Bas *et al.*, 1986; Cantagrel *et al.*, 1993). The lower part of the subaerial volcanic series, also unaffected by the ductile episode, has been dated at 22 Ma (Coello *et al.*, 1991; Ancochea *et al.*, 1993; Balcells *et al.*, 1994). Therefore, the age of the ductile deformational events may be established as Late Oligocene to Early Miocene.

Some relevant data for the interpretation of the tectonic regime that governed the activity of these shear zones have been obtained in the PPBSZ. As stated above, four sets of type 2 albitite veins are arranged in an almost orthorhombic pattern (Fig. 6b). Several authors proposed similar patterns to explain the kinematics of brittle fractures in a context of bulk non-plane deformation (e.g. Oertel, 1965; Reches, 1983; Reches and Dieterich, 1983). This concept is convincingly applied by Kirschner and Teyssier (1994) to coeval, orthorhombically arranged, en échelon vein arrays. The albitite veins in Punta del Peñón Blanco are not en échelon arrays. However, field criteria show that they accommodated some displacement parallel to the vein boundary, even though the main component is of vein-perpendicular extension. The cross-cutting relationships between the four sets suggest that they formed simultaneously. Furthermore, three lines of evidence reinforce the association between the type 2 veins and the ductile shear zones. First, the veins always appear in the immediate neighbourhood to the ductile shear zones. Second, representative orientation of the mylonitic foliation in the PPBSZ, coincide with one of the vein sets (Fig. 11a). Lastly, the orientation of minor

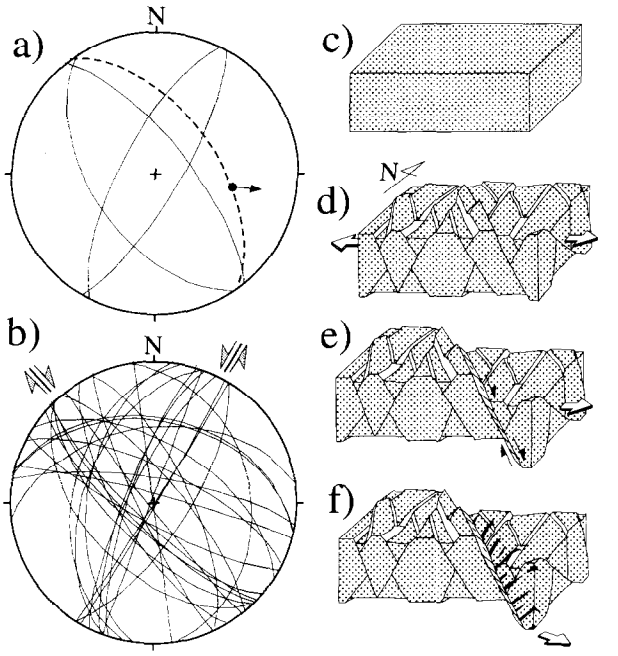

Fig. 11. (a) Equal area, lower hemisphere projection of the type 2 albitite veins of the Punta del Peñón Blanco fractured area (thin great circles); also shown are the average orientation of the foliation (dashed great circle) and stretching lineation (black dot, the arrow indicates the shear sense) in the ductile PPBSZ. (b) Equal area, lower hemisphere projection of dextral and sinistral ductile shear zones in the Basal Complex, excluding the Caleta de la Cruz and Punta del Peñón Blanco shear zones. (c) to (f) Hypothetical model for the tectonic evolution of the ductile–brittle shear zones in the Fuerteventura Basal Complex. Carbonatites and syenites are not distinguished.

ductile shear zones outside the CCSZ and PPBSZ show four sets that closely fit the pattern of the albitite veins (Fig. 11b). Interestingly, the NW-trending shear zones are consistently dextral to normal-dextral, and the NE-trending ones are sinistral to normal-sinistral. Furthermore, the minor shear zones related to the main PPBSZ present a similar configuration (Fig. 7a & b).

Accordingly, we propose the following kinematic scenario for the development of ductile shear zones in the Basal Complex of Fuerteventura (Fig. 11c–f).

(1) After the intrusion of large pyroxenite bodies and small syenite stocks (Fig. 11c) into a sedimentary and submarine volcanic series, a bulk extensional deformation began to affect these rocks. The finite deformation ellipsoid was of the general flattening type (Ramsay and Huber, 1983). The short axis of the ellipsoid was vertical, and the trend of the long and intermediate principal axes (both horizontal and implying positive elongation) was E–W and N–S, respectively. A high fluid-pressure (alkaline fluids) may have contributed to the brittle fracturing of the pyroxenite, first as a network of albitite, and then as a system of four sets of orthorhombically arranged veins (Fig. 11d). These alkaline fluids are derived through fenitization from ascending carbonatite magmas (Le Bas, 1984).

(2) Final intrusion of carbonatite magma and nepheline syenite dykes led to a rheological threshold, with the

onset of ductile deformation and large shear displacements along one or several of the previous four sets of fractures (Fig. 11e).

(3) Finally, during the waning stages of the tectonic activity, the deformation was concentrated in the hanging-wall block, with the development of tensional fractures normal to the slip vector (stretching lineation). The fluid pressure associated with the syenitic intrusions was high enough to collaborate in the development of these fractures, that became filled with the type 3 white syenite veins. They occasionally traversed the ductile fabrics at the top of the shear bands (Fig. 11f).

This model would account adequately for the observations in the Punta del Peñón Blanco area.

Giant submarine slides related to the gravitational collapse of large volcanoes have been described by Lipman *et al.* (1988) and Moore *et al.* (1995) on the west flank of the island of Hawaii. The collapse was associated to the activity of listric normal faults limiting large block-slumps in the breakaway area, and to dyke injection (Lipman *et al.*, 1988). Similarities between Fuerteventura and those collapse structures in Hawaii rely on the extensional character of the deformation. However, there are several important differences. First, the listric faults in Hawaii are thin-skinned gravity driven features that only affect the oversteepened accumulation of volcanic material (see Fig. 4 of Moore *et al.*, 1995). However, the mantle origin of the melts and alkaline fluids related to the tectonic activity of Fuerteventura, and the large displacements verified along the ductile shear zones suggest that these may be large structures of a lithosphere scale. Secondly, rapid (catastrophic) movement is advocated by Moore *et al.* (1995) to explain the characteristics of the Hawaiian slumps. The structures in the shear zones of Fuerteventura clearly need lower strain rates to develop. Thirdly, the extensional tectonics of Fuerteventura is not a local and episodic feature. The influence of this extensional regime is evident also in more recent structures, such as the dyke-swarm that traverses the Basal Complex in Fuerteventura (e.g. Stillman *et al.*, 1975; Stillman, 1987), the fracture systems in Lanzarote (Marinori and Pasquarè, 1994), or the structures recognized to the north and south of the Canary archipelago by Dañobeitia and Collette (1989). This implies similarly oriented structures covering an area with a length of several hundred of km. Furthermore, it is long-lived tectonics, lasting from at least the Upper Oligocene to the present. Fourthly, several local collapse features resembling the Hawaiian landslides have been proposed for the subaerial volcanoes of Fuerteventura by Ancochea *et al.* (1993). Current work is devoted to distinguishing the structures related to these local collapses. In brief, the explanation of the Fuerteventura tectonics must rely on a larger, lithospheric scale.

The upper mantle below the eastern Atlantic, and western and central Europe may be influenced by a large-scale mantle upwelling region, as suggested by Hoernle *et al.* (1995). Furthermore, Neumann *et al.* (1995) proposed a thinned lithosphere beneath the eastern Canary Islands according to their study on mantle xenoliths from Lanzarote. The NE–SW elongate region of upwelling in the eastern Atlantic may be responsible for the uplift and rifting of the lithosphere, the shear zones acting as structures that accommodated vertical displacements and horizontal extension in an E–W to WNW–ESE direction (and also in a N–S direction). At the same time, these structures served as ascent channels for magmas of a deep origin in the mantle. This idea of a rifting in the Canary Islands is not new, having already been cited by Stillman *et al.* (1975).

Cannat *et al.* (1991) described similar structures in the Southwest Indian Ridge (ODP leg 118, site 735), with mylonitic shear zones and syntectonic magmatic intrusions. They relate these structures with the tectonics in slow-spreading oceanic ridges. Paleo-spreading centres in the Oman ophiolite are interpreted as the site of ascent of mantle diapirs emerging on the paleo-ridge axis (Ceuleneer, 1991), thus demonstrating the importance of the mantle upwellings in the tectonics of their overlying lithosphere. Clearly, the Fuerteventura case is one of intraplate tectonics, and the rifting process, slow and long-lasting, never produced the growth of oceanic crust with MORB signatures. However, the mechanism triggering the extension (large-scale mantle anomalies) and the structures developed are similar to those found in active or fossil ridge segments. Another important, although hitherto unexplained, issue is the relationship between this tectonic activity and the plate tectonics framework in the northwest corner of the African plate.

CONCLUSIONS

A system of ductile shear zones affected the Basal Complex of Fuerteventura from the Late Oligocene to the Early Miocene. Within the ultra-alkaline pyroxenites they began as brittle structures, associated with the ascent of alkaline magma and related fluids. These led to substantial mineral changes in the pyroxenites, which became rich in sheet-silicates and were traversed by carbonatites and syenites. Temperatures of around 500 °C were reached along these structures. A rheological change toward ductile deformation followed. This generated a large number of meso- and microstructures, as well as strong crystallographic fabrics. Two main ductile shear bands have been identified and described in this work: the Caleta de la Cruz and the Punta del Peñón Blanco shear zones.

Kinematically, these shear zones are high-angle extensional structures with variable strike-slip components. Displacements may well exceed 1 km in some cases. Both within individual fractured areas (Punta del Peñón Blanco) and as a geometrical feature of the deformed Basal Complex as a whole, the shear zones present a

nearly orthorhombic arrangement. In accordance with the interpretation given in the literature to other similar structures, a model of bulk irrotational, non-planar deformation is applied to these structures. Two principal axes of finite strain appear within the horizontal plane: the maximum positive elongation occurred in an E–W direction, with a minor extension along the N–S axis.

These geometrical and kinematical considerations, together with the magmatic context in which the shear zones were active, suggest a rifting scenario. The presence of large upwelling instability within the mantle under the African lithosphere may partly explain this tectonic activity. The complex plate-tectonics interplay between the Eurasian and African plates must be also considered, even if its influence seems more difficult to evaluate.

The development of major ductile shear zones is not exclusive to or characteristic of the continents; it may also be a conspicuous feature of the oceanic crust, not just at the plate boundaries but also in relation to intraplate tectonic activity.

Acknowledgements—We would like to thank R. Arenas for comments and fruitful discussions. The Cabildo Insular de Fuerteventura and Tercio III de La Legión considerably facilitated the field work. We thank A. Robertson and M. J. Le Bas for their constructive reviews of the manuscript. This study was supported by the CICYT (Projects PB91-0147-CO2-02 and P1394-0596) and the Junta de Andalucía (PAI 4108).

REFERENCES

Abdel-Monem, A., Watkins, N. D. and Gast, P. W. (1971) Potassium–argon ages, volcanic stratigraphy, and geomagnetic polarity history of the Canary Islands: Lanzarote, Fuerteventura, Gran Canaria and La Gomera. *American Journal of Science* **271**, 490–521.

Allerton, S. and Vine, F. J. (1992) Deformation styles adjacent to transform faults: evidence from the Troodos ophiolite, Cyprus. In *Ophiolites and their Modern Oceanic Analogues* eds L. M. Parson, B. J. Murton, and P. Browning *Special Publications of the Geological Society London* **60**, 251–261.

Ancochea, E., Fúster, J. M., Ibarrola, E., Cendrero, A., Coello, L., Herndán, F., Cantagrel, J. M. and Jamond, C. (1990) Volcanic evolution of the Fuerteventura Island in the light of new K–Ar data. *Journal of Volcanology and Geothermal Research* **44**, 231–249.

Ancochea, E., Brändle, J. L., Cubas, C., Hernán, F. and Huertas, M. (1993). La Serie I de la isla de Fuerteventura. *Memorias de la Real Academia de Ciencas Exactes, Física y Naturales de Madrid* **27**, 1–151.

Ancochea, E., Hernán, F., Cendrero, A., Cantagrel, J. M., Fúster, J. M., Ibarrola, E. and Coello, J. (1994) Constructive and destructive episodes in the building of a young oceanic island, La Palma, Canary Islands and genesis of the Caldera de Taburiente. *Journal of Volcanology and Geothermal Research* **60**, 243–262.

Argus, D. F., Gordon, R. G., DeMets, C. and Stein, S. (1989) Closure of the Africa–Eurasia–North America plate motion circuit and tectonics of the Gloria fault. *Journal of Geophysical Research* **94**(B5), 5585–5602.

Balcells, R., Barrera, J. L., Gómez, J. A., Cueto, L. A., Ancochea, E., Huertas, M. L., Ibarrola, E. and Snelling, N. (1994) Edades radiométricas de los edificios miocenos de Fuerteventura (Islas Canarias). *Boletín geológico y minero* **105**, 50–56.

Banda, E., Dañobeitia, J. J., Suriñach, E. and Ansorge, J. (1981) Features of crustal structure under the Canary Islands. *Earth and Planetary Science Letters* **55**, 11–24.

Berthé, D., Choukroune, P. and Jegouzo, P. (1979) Orthogneiss, mylonite and non coaxial deformation of granites: the example of the South Armorican Shear Zone. *Journal of Structural Geology* **1**, 31–42.

Buforn, E., Udías, A. and Colombás, M. A. (1988) Seismicity, source mechanisms and tectonics of the Azores–Gibraltar plate boundary. *Tectonophysics* **152**, 89–118.

Cannat, M., Mével, C. and Stakes, D. (1991) Stretching of the deep crust at the slow-spreading Southwest Indian Ridge. *Tectonophysics* **190**, 73–94.

Cantagrel, J. M., Fúster, J. M., Pin, C., Renaud, U. and Ibarrola, E. (1993) Age Miocène inférieur des carbonatites de Fuerteventura. *Comptes Rendue de l'Académie des Sciences de Paris* **316**, 1147–1153.

Casillas, R., Ahijado, A. and Hernández-Pacheco, A. (1994) Zonas de cizalla dúctil en el Complejo Basal de Fuerteventura. *Geogaceta* **15**, 117–120.

Chase, C. G. (1978) Plate kinematics: The Americas, East Africa and the rest of the world. *Earth and Planetary Science Letters* **37**, 355–368.

Ceuleneer, G. (1991) Evidence for a paleo-spreading center in the Oman ophiolite: mantle structures in the Maqsad area. In *Ophiolite Genesis and Evolution of the Oceanic Lithosphere* eds. A. Peters, A. Nicolas and R. G. Coleman, pp. 147–173. Kluwer, Dordrecht.

Coello, L., Cantagrel, J. M., Hernán, F., Fúster, J. M., Ibarrola, E., Ancochea, E., Casquet, C. and Jamond, C. (1991) Evolution of the eastern volcanic ridge of the Canary Islands based on new K–Ar data. *Journal of Volcanology and Geothermal Research* **53**, 251–274.

Dañobeitia, J. J. and Collette, B. J. (1989) Estudio mediante sísmica de reflexión de un grupo de estructuras submarinas situadas al Norte y Sur del archipiélago Canario. *Acta Geologica Hisp.* **24**, 147–163.

Fairbairn, H. W. (1941) Petrofabric relations of nepheline and albite in litchfieldite from Blue Mountain, Ontario. *American Mineralogist* **26**, 316–320.

Fjäder, K., Gudmundsson, A. and Forslund, T. (1994) Dikes, minor faults and mineral veins associated with a transform fault in North Iceland. *Journal of Structural Geology* **16**, 109–119.

Fúster, J. M. and Aguilar, M. (1965) Nota previa sobre la geología del Macizo de Betancuria, Fuerteventura (Islas Canarias). *Estudios Geologicos* **21**, 181–197.

Fúster, J. M., Muñoz, M., Sagredo, L., Yébenes, A., Bravo, T. and Hernández-Pacheco, A. (1980) Excursión n° 121 A + c del 26° I. G. C. a las Islas Canarias. *Boletín Instituto geológico Minero España.* **92**, 351–390.

Grunau, H. R., Lehner, P., Cleintaur, M. R., Allenbach, P. and Bakker, G. (1975) New radiometric ages and seismic data from Fuerteventura (Canary Islands), Maio (Cape Verde Islands) and Sao Tomé (Gulf of Guinea). In *Progress in Geodynamics. Royal Soc. Neth. Acad. Arts Sci.* pp. 335–352. Amsterdam.

Gudmundsson, A. (1992) Formation and growth of normal faults at the divergent plate boundary in Iceland. *Terra Nova* **4**, 464–471.

Hansen, E. (1971) *Strain Facies*. Springer-Verlag, Berlin.

Hoernle, K., Zhang, Y.-S. and Graham, D. (1995) Seismic and geochemical evidence for large-scale mantle upwelling beneath the eastern Atlantic and western and central Europe. *Nature* **374**, 34–39.

Javoy, M., Stillman, C. J. and Pineau, F. (1986) Oxygen and Hydrogen isotope studies on the Basal Complexes of the Canary Islands. *Contributions to Mineralogy and Petrology* **92**, 225–235.

Kirschner, D. L. and Teyssier, C. (1994) Orthorhombically arranged vein arrays. *Journal of Structural Geology* **16**, 1129–1138.

Law, R. D. (1990) Crystallographic fabrics: a selective review of their applications to research in structural geology. In *Deformation Mechanisms, Rheology and Tectonics* eds R. J. Knipe and E. H. Rutter, *Special Publications of the geological Society London.* **54**, pp. 335–352

Le Bas, M. L. (1984) Oceanic carbonatites. In *Kimberlites and Related Rocks*, ed. L. Kornprobst, pp. 169–178. Elsevier, Amsterdam.

Le Bas, M. J., Rex, D. C. and Stillman, C. J. (1986) The early magmatic chronology of Fuerteventura. *Geological Magazine* **123**, 287–298.

Lipman, P. W., Normark, W. P., Moore, J. G., Wilson, J. B. and Gutmacher, C. E. (1988) The giant submarine Alika debris slide, Mauna Loa, Hawaii. *Journal of Geophysical Research* **93**, 4279–4299.

MacLeod, C. J. and Murton, B. J. (1993) Structure and tectonic evolution of the Southern Troodos Transform Fault Zone, Cyprus. In *Magmatic Processes and Plate Tectonics*, eds H. M. Prichard, T. Alabaster, N. B. W. Harris and C. R. Neary, *Special Publications of the Geological Society, London.* **76**, pp. 141–176.

Marinoni, L. B. and Pasquarè, G. (1994) Tectonic evolution of the emergent part of a volcanic ocean island: Lanzarote, Canary Islands. *Tectonophysics* **239**, 111–135.

Meco, J. and Pomel, R. (1985) Les formations marines et continentales intravolcaniques des Iles Canaries Orientales (Grande Canaria,

Fuerteventura et Lanzarote): Stratigraphie et signification paléoclimatique. *Estudios Geológicos* **41**, 223–228.

Mercier, J.-C. C. (1985) Olivine and pyroxenes. In *Preferred Orientation in Deformed Metals and Rocks: an Introduction to Modern Texture Analysis*, ed. K.-R. Wenk, pp. 407–430. Academic Press, Orlando.

Minster, J. B. and Jordan, T. H. (1978) Present-day plate motions. *Journal of Geophysical Research* **83**(B11), 5331–5354.

Moore, J. G., Bryan, W. B., Beeson, M. H. and Normark, W. R. (1995) Giant blocks in the South Kona landslide, Hawaii. *Geology* **23**, 125–128.

Moreira, V. S. (1991) Historical seismicity and seismotectonics of the area situated between the Iberian Peninsula, Morocco, Selvagens and Azores Islands. In *Seismicity, Seismotectonics and Seismic Risk of the Ibero–Maghrebian Region*, ed. J. Mezcua and A. Udías, *Publicaciones del Instituto Geográfico Nacional*. Vol. **8**, pp. 213–225.

Morgan, W. J. (1983) Hotspot tracks and the early rifting fo the Atlantic. *Tectonophysics* **94**, 123–139.

Müller, R. D., Royer, J.-Y. and Lawver, L. A. (1993) Revised plate motions relative to the hotspots from combined Atlantic and Indian Ocean hotspot tracks. *Geology* **21**, 275–278.

Neumann, E.-R., Wulff-Pedersen, E., Johnsen, K., Andersen, T. and Krogh, E. (1995) Petrogenesis of spinel harzburgite and dunite suite xenoliths from Lanzarote, eastern Canary Islands: Implications for the upper mantle. *Lithos* **35**, 83–107.

Nicolas, A. (1989) *Structure of Ophiolites and Dynamics of Oceanic Lithosphere*. Kluwer, Dordrecht.

Oertel, G. (1965) The mechanism of faulting in clay experiments. *Tectonophysics* **2**, 343–393.

Passchier, C. W. and Simpson, C. (1986) Porphyroclast systems as kinematic indicators. *Journal of Structural Geology* **8**, 831–843.

Ramsay, J. G. and Huber, M. (1983) *The Techniques of Modern Structural Geology, Strain Analysis*, **Vol. 1**, Academic Press, London.

Reches, Z. (1983) Faulting of rocks in three-dimensional strain fields II; Theoretical analysis. *Tectonophysics* **95**, 133–156.

Reches, Z. and Dieterich, J. (1983) Faulting of rocks in three-dimensional strain fields I. Failure of rocks in polyaxial, servo-control experiments. *Tectonophysics* **95**, 111–132.

Renz, O., Bernouilli, D. and Hottinger, L. (1992) Cretaceous ammonites from Fuerteventura, Canary Islands. *Geological Magazine* **129**, 763–769.

Robertson, A. H. F. and Bernouilli, D. (1982) Stratigraphy, facies and significance of Late Mesozoic and Early Tertiary sedimentary rocks of Fuerteventura (Canary Islands) and Maio (Cape Verde Islands). In *Geology of the Northwest African Continental Margin*, eds U. Von Rad, K. Hinz, M. Sarnthein and E. Seibold, pp. 498–525. Springer-Verlag, Berlin.

Robertson, A. H. F. and Stillman, C. J. (1979) Late Mesozoic sedimentary rocks of Fuerteventura, Canary Islands. Implications for West Africa continental margin evolution. *Journal of Geological Society London* **136**, 47–60.

Robertson, A. H. F. and Stillman, C. J. (1979) Submarine volcanic and associated sedimentary rocks of the Fuerteventura Basal Complex, Canary Islands. *Geological Magazine* **116**, 203–214.

Rothe, P. (1968) Mesozoische Flysch-Alblagerugen auf der Kanareninsel Fuerteventura. *Geologische Rundschau* **58**, 314–332.

Sacerdoti, M., Labernadiere, H. and Gandais, M. (1980) Transmission electron microscope (TEM) study of geologically deformed potassic feldspars. *Bulletin Mineralogique* **103**, 155–158.

Sagredo, L, Ancochea, E., Brändle, J. L., Cubas, C. R., Fúster, J. M., Hernández-Pacheco, A. and Muñoz, M. (1989) Magmatismo hipoabisal-subvolánico y vulcanismo en un ámbito geodinámico distensivo (Fuerteventura, Islas Canarias). Meeting on Canarian Volcanism. Lanzarote Abstracts (European Science Foundation). pp. 100–103.

Scandale, E., Gandais, M. and Willaime, C. (1983) Transmission electron microscopy study of experimentally deformed K-feldspar single crystals. The (010)[001], (001)112[110], (110)1/2[112] and (111)1/2[110] slip systems. *Physics and Chemistry of Minerals* **9**, 182–187.

Schmid, S., Panozzo, R. and Batier, S. (1987) Simple shear experiments on calcite rocks: rheology and microfabric. *Journal of Structural Geology* **9**, 747–778.

Schmincke, H. U. (1982) Volcanic and chemical evolution of the Canary Islands. In *Geology of the Northwest African Continental Margin*, eds U. Von Rad, K. Hinz, M. Sarnthein and E. Seibold, pp. 274-306. Springer-Verlag, Berlin.

Smith, J. V. and Brown, W. L. (1988) *Feldspar Minerals*. Crystal Structures, Physical, Chemical and Microtextural Properties, **Vol 1**, Springer-Verlag, Berlin.

Staudigel, H. and Schmincke, H. U. (1984) The Pliocene seamount series of La Palma, Canary Islands. *Journal of Geophysical Research* **89**(B13), 11195–11215.

Stillman, C. J. (1987) A Canary Islands dyke swarm: Implications for the formation of oceanic islands by extensional fissural volcanism. In *Mafic Dyke Swarms*, eds H. C. Halls and W. R. Fahrig, *Geological Association of Canada Special Paper* **34**, pp. 243–255.

Stillman, C. J., Fúster, J. M., Bennell-Baker, M. J., Muñoz, M., Smewing, J. D. and Sagredo, J. (1975) Basal Complex of Fuerteventura (Canary Islands) as an oceanic intrusive complex with rift-system affinities. *Nature* **257**, 469–471.

Sturt, B. A. (1961) Preferred orientation of nepheline in deformed nepheline syenite gneisses from Sørøy, northern Norway. *Geological Magazine* **98**, 464–467.

Taylor, B. E. and Liou, J. G. (1978) The low-temperature stability of andradite in C–O–H fluids. *American Mineralogy* **63**, 378–393.

Turner, F. J. and Weiss, L. E. (1963) Structural Analysis of Metamorphic Tectonites. McGraw-Hill, New York.

Varga, R. J. (1991) Modes of extension at oceanic spreading centers: evidence from the Solea graben, Troodos ophiolite, Cyprus. *Journal of Structural Geology* **13**, 517–537.

Vegas, R. (1985) Tectónica del área Ibero-Mogrebí. In *Mecanismo de los terremotos y tectónica* eds A. Udías, D. Muñoz and E. Buforn, pp. 197-215. Universidad Complutense de Madrid.

Villemin, T., Bergerat, R., Angelier, J. and Lacasse, C. (1994) Brittle deformation and fracture patterns on oceanic rift shoulders: the Esja peninsula, SW Iceland. *Journal of Structural Geology* **16**, 1641–1654.

Weijermars, R. (1988) Where does Africa meet Europe? *Nature* **332**, 118.

Westaway, R. (1990) Present-day kinematics of the plate-boundary zone between Africa and Europe, from the Azores to the Aegean. *Earth and Planetary Science Letters* **96**, 393–406.

Wenk, H.-R. and Christie, J. M. (1991) Comments on the interpretation of deformation textures in rocks. *Journal of Structural Geology* **13**, 1091–1110.

White, S. H. and Knipe, R. P. (1978) Transformation-and reaction-enhanced ductility in rocks. *Journal of Geological Society London* **135**, 513–516.

Willaime, C., Christie, J. M. and Kovacs, M.-P. (1979) Experimental deformation of K-feldspar single crystals. *Bulletin Mineralogy* **102**, 168–177.